Geophys. J. Int. (2006) **167,** 570–584 doi: 10.1111/j.1365-246X.2006.03184.x

Water volume change in the lower Mekong from satellite altimetry and imagery data

F. Frappart,[1,2] K. Do Minh,[1] J. L'Hermitte,[3] A. Cazenave,[1] G. Ramillien,[1] T. Le Toan[3] and N. Mognard-Campbell[1]

[1] *Laboratoire d'Etudes en Géophysique et Océanographie Spatiales (LEGOS), Observatoire Midi-Pyrénées, UMR* 5566, *CNES/CNRS/IRD/UPS,* 14 *Av. Edouard Belin,* 31400 *Toulouse, France. E-mail: frederic.frappart@legos.cnes.fr*

[2] *Laboratoire des Mécanismes et Transferts en Géophysique (LMTG), Observatoire Midi-Pyrénées, UMR* 5563, *CNRS/IRD/UPS,* 14 *Av. Edouard Belin,* 31400 *Toulouse, France*

[3] *Centre d'Etudes Spatiales de la BIOsphère (CESBIO), Observatoire Midi-Pyrénées, UMR* 5126, *CNES/CNRS/IRD/UPS,* 18 *Av. Edouard Belin,* 31401 *Toulouse Cedex* 9, *France*

Accepted 2006 August 7. Received 2006 August 7; in original form 2005 November 2

SUMMARY

We have analysed satellite altimetry data from the ERS-2, ENVISAT and Topex/Poseidon satellites to construct water level time-series over a 8 yr period (from 1996 April to 2004 April) over the lower Mekong river basin. The study area includes the Tonle Sap Lake, seasonally inundated areas and several branches of the hydrographic network of the Mekong delta. We found a very strong seasonal signal over the main river north of 13°N, the Tonle Sap Lake and Tonle Sap river, with amplitudes reaching 8–10 m annually. We also found a clear interannual signal in altimetry-derived water level time-series. For example, year 1999 had weak floods (around 6 m amplitude), contrasting with year 2000 during which strong flood was noticed (around 10 m amplitude). Southwards, we also observed large seasonal fluctuations (2–3 m) over inundated floodplains, as identified using satellite imagery data from the SPOT-4 Vegetation instrument. Depending on the location, quite different annual amplitudes were observed, the closer to the Mekong mouth, the smaller the signal (less than 0.5 m seasonal amplitude). Using Normalized Difference Vegetation Index (NDVI) data from the Vegetation instrument, we studied the seasonal extent of flood plains in the delta. Then combining the areal extent of floods with water levels estimated from the ERS-2/ENVISAT data, we computed maps of monthly surface water volume change over six successive years (1998–2003), the period of availability of the NDVI data. Averaged over the lower Mekong basin, this surface water volume change was then compared to the total (i.e. surface plus underground) water volume change inferred from the GRACE satellite. They exhibit in-phase fluctuations.

Key words: multispectral imagery, radar altimetry, water volume change.

1 INTRODUCTION

The Mekong river basin is one of the largest of the world, climatically controlled, but with some anthropogenic alterations, especially in the lower part and in the delta [Mekong River Commission (MRC) 2005]. The annual recurrence of the monsoon floods in the Cambodian floodplains, from August to November, is of great importance for farming and economic activity. Between 80 and 90 per cent of the freshwater use in the Mekong basin is for irrigating rice crops (MRC 2002). In some years, vast regions are flooded for several weeks, causing serious damage. The year 2000, for instance, was characterized by a particularly severe flood, reported as the most devastating in the last 40 yr (Dutta & Takeuchi 2000; MRC 2005).

Water storage in wetlands and corresponding outflow represent a significant part of the water balance of large river basins (Alsdorf *et al.* 2001). To better understand the hydrology of large river systems, information about the dynamics of inundation patterns (extent of flooded areas) and water levels of main river channels, tributaries and associated floodplains is required (Alsdorf *et al.* 2000).

Spatial and temporal patterns of inundation areas have been inferred from multitemporal satellite visible/infrared images, Synthetic Aperture Radar sensors or microwave radiometers (Mertes *et al.* 1995; Smith 1997; Sippel *et al.* 1998; Töyrä *et al.* 2001; Hess *et al.* 2003). In South America, inundation patterns of large floodplains have been derived using the polarization difference at 37 GHz of the scanning multichannel microwave radiometer (SMMR) passive microwave emission measurements (ground resolution of 0.25°) (Hamilton *et al.* 2002). Relations between stage and flooded area have been derived using records from *in situ* gauge stations (Sippel *et al.* 1998).

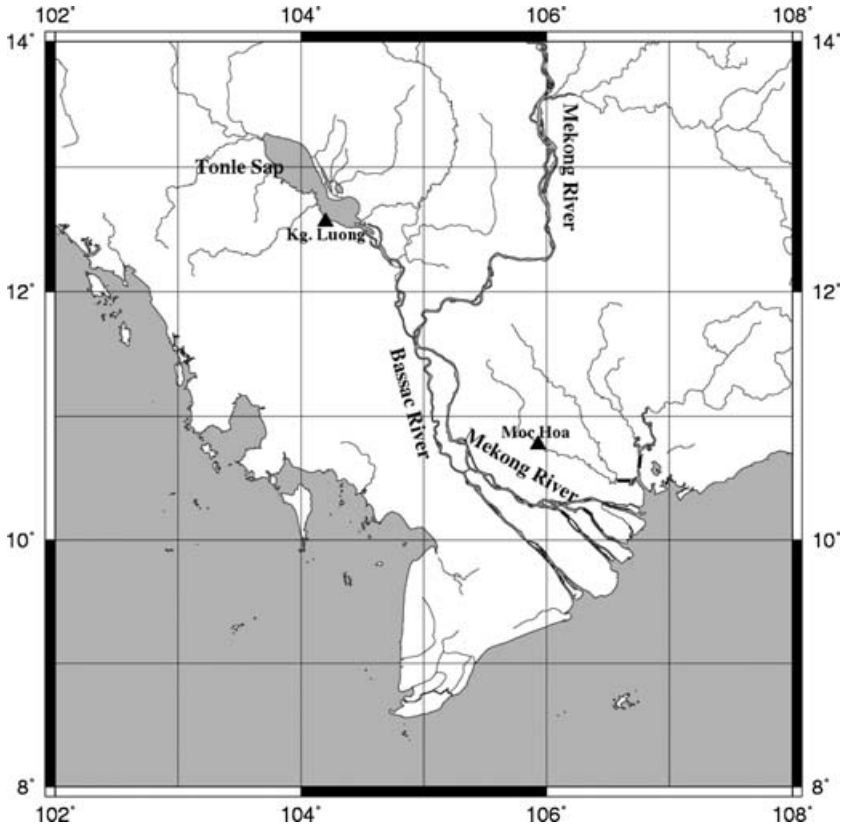

Figure 1. Map of the Mekong basin. The black triangles represent the *in situ* gauge stations.

Hydrological models have been used to determine the extent of flooded areas too. For instance, in the Amazon basin, the extension of the inundated areas was determined using a terrestrial ecosystem model (integrated biosphere simulator—IBIS) and a hydrological routing algorithm (HYDRA) by Coe *et al.* (2002).

In the lower Mekong basin, the flood extent has been studied using satellite imagery from quick-look mosaics of the SPOT satellite (Chia *et al.* 2001) and the Special Sensor Microwave/Imager (SSM/I) (Tanaka *et al.* 2003). The complete hydrological state of the Mekong river and its tributaries was simulated for the period 1994–1998 (Kite 2001). This study provided an estimate of the total outflow of the Mekong basin and area of land flooded by Tonle Sap river.

Recently, a new methodology, based on the combined use of radar altimetry and satellite imagery, was developed to determine volume variations of surface water in the Negro river basin, the main tributary of the Amazon river (Frappart *et al.* 2005).

In the present study, we apply a similar method to monitor the volume variation of surface water during seasonal floods (August to December) in the lower Mekong basin over a 6 yr period (1998–2003), using multispectral imagery from the Vegetation instrument onboard the SPOT-4 satellite and altimetry-derived water levels from the Topex/Poseidon (T/P), ERS-2 and ENVISAT satellites.

2 HYDROLOGICAL CHARACTERISTICS OF THE STUDY AREA

The Mekong basin is the largest river basin in South East Asia with an area of 795 000 km^2 [Interim Mekong Committee (IMC) 1988]. It is the home for over 65 millions inhabitants (MRC 1997). The Mekong river has its source on the Tibetan Plateau and then flows through six countries (China, Burma, Laos, Thailand, Cambodia and Vietnam) before reaching the South China Sea. With a mean annual flow of 475 000 m^3 and a total length 4800 km, it is the world's 10th greatest and 12th longest, respectively (IMC 1988). The lower Mekong basin which drains a total catchment area of 606 000 km^2 (77 per cent of the basin), is considered as the most important part of the Mekong basin, both environmentally and economically (IMC 1988; Hori 2000). The study area is the lower Mekong river basin and delta. At Phnom Penh (Cambodia), the Mekong river divides into three parts: the Tonle Sap river, the Bassac river and the lower Mekong. During the flood season, water is drained from the Mekong and Bassac rivers into the Tonle Sap Lake, through the Tonle Sap river, and when the water level decreases in the Mekong river, the water is drained from the Tonle Sap Lake into the Mekong and Bassac rivers. The reversal of the flow of the Tonle Sap river is a unique hydrological feature that is responsible for a higher dry season flow in the delta than if it only received water from the Mekong river (Hoanh *et al.* 2003). When reaching the Vietnam border, the main river divides into several branches which constitute the Mekong delta. This region is very flat (less than 100 m elevation) and is referred as the Mekong lowlands (MRC 2003). Fig. 1 is a sketch of the study area.

The hydrological regime of the Mekong river is primarily dependent on the climatic conditions of the alternating wet and dry seasons. Climate is governed by the monsoon winds that blow northeast or southwest depending on the period of the year. The southwest monsoon corresponds to the rainy season which ranges from May to October, with a peak in September. To depict the precipitation

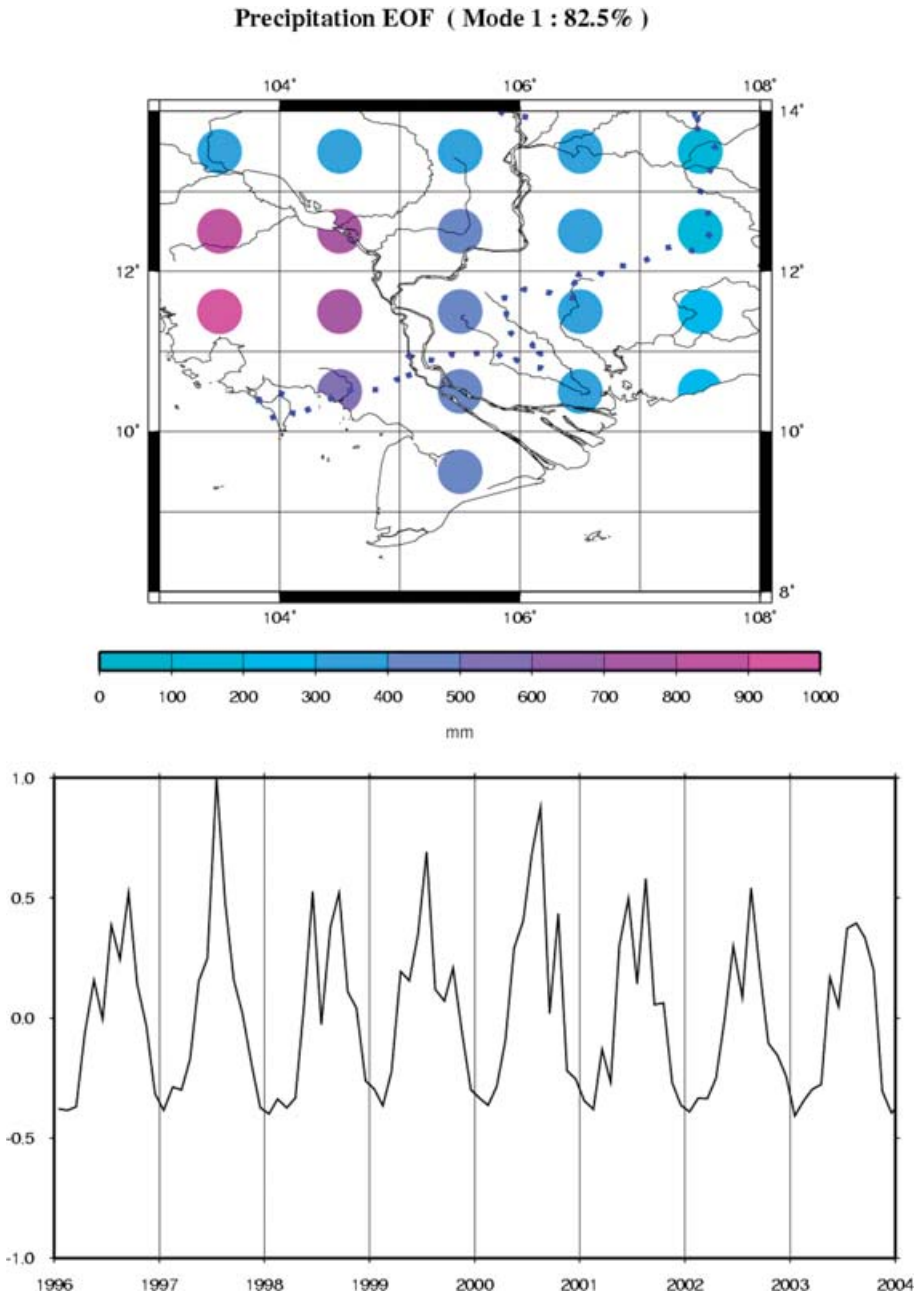

Figure 2. Mode 1 of the EOF decomposition of precipitation from GPCC (Rudolf *et al.* 1994, 2003) over the lower Mekong, between 1996 and 2003. The upper panel represents the spatial mode whereas the lower panel represents the temporal variation of the precipitation. The percentage of variance explained by the first mode is 82.5 per cent.

patterns over the study area, we have applied empirical orthogonal functions (EOF) decomposition, based on Lanczos orthogonalizations and singular value decompositions (SVD) of large linear systems (e.g. Toumazou & Crétaux 2001), to precipitation data. The data used here are monthly $1^\circ \times 1^\circ$ gridded precipitation of the Global Precipitation Climate Center based on quality-controlled data from 7000 stations (Rudolf *et al.* 1994, 2003). Fig. 2 shows the leading mode of the EOF decomposition of precipitation data over the lower Mekong, over the 8 yr period of analysis (1996 April to 2004 April). The temporal curve shows a clear annual cycle, peaking in September. As indicated by the spatial pattern map, the wettest region is the southern uplands and lowlands, south of the Tonle Sap Lake and northern part of the delta.

Superimposed on the annual cycle, some interannual fluctuations are visible. Fig. 2 indicates two particularly rainy years: 1997 and 2000. The lowlands suffer annual floods during the rainy season. During the rainy year 2000, a particularly devastating flood affected a very large area. This event will be discussed below in some detail.

3 SATELLITE DATA SETS

In this study, we use different satellite data sets: radar altimetry data from the T/P, ERS-2 and ENVISAT satellites for measuring water level changes, and Normalized Difference Vegetation Index (NDVI)

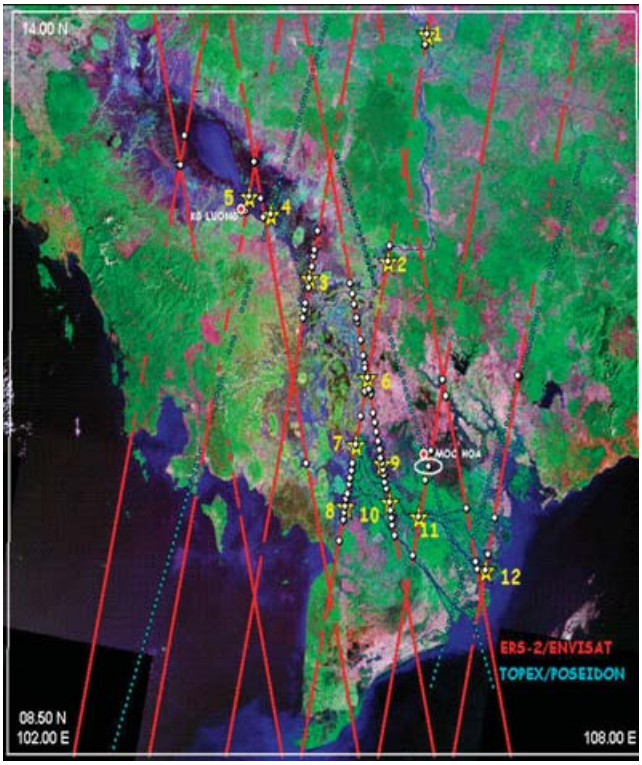

Figure 3. Spatial coverage of radar altimeters over the Mekong basin. The red lines correspond to ERS-2/ENVISAT tracks, the light blue dotted lines correspond to T/P tracks. The 80 virtual stations are represented using white dots, the yellow stars correspond to the ones presented in Fig. 6. The red circles with a white border represent the *in situ* gauge stations. The white ellipse corresponds to the intersection between T/P and ERS-2/ENVISAT tracks.

data from the Vegetation instrument onboard the SPOT-4 satellite to determine the surface water extent over inundated plains.

3.1 ERS-2, ENVISAT and Topex/Poseidon altimetry data

ERS-2, launched in 1995 by the European Space Agency (ESA), is the successor of ERS-1, designed to study the Earth's environment. The satellite carries, among other instruments, a radar altimeter developed for measuring sea surface height. However, retracking of the raw altimeter waveforms (radar echoes) allows the use of the ERS data over continental surface waters (Legrésy 1995). Here we only use the ERS-2 retracked altimetry data because the ERS-1 retracked data suffer too many gaps. The ERS-2 altimetry time-series (20 Hz data—corresponding to an along-track ground resolution of about 300 m) used here starts in 1996 April. The average intertrack spacing over the lower Mekong basin is 85 km, while the revisit time (orbital cycle) is 35 days. The ENVISAT satellite was launched on 2002 February by ESA for environmental objectives (Gardini *et al.* 1995). The satellite's payload includes a radar altimeter operating at two frequencies. Its orbital characteristics are similar to those of the ERS satellites (i.e. same repeat cycle and ground-track spacing). The ENVISAT altimeter provides radar echoes over ocean, land and ice to measure sea surface height, surface water level variations over river basins and ice surface elevation (Wehr & Attema 2001). For the ENVISAT mission, four different algorithms are operationally applied to radar echo data to provide altimeter height estimates (Zelli 1999): each of them has been developed for a specific surface response. One for ocean (ESA 2002), two for ice sheets (Bamber 1994; Legrésy 1995) and one for sea ice (Laxon 1994). In this study, we use the ENVISAT 20 Hz height measurements contained in the geophysical data records (GDRs) (ESA 2002) from cycle 2002/09/12 to 2004/04/10 of ENVISAT Mission. For the ENVISAT data, we use the range measurements processed with the offset centre of gravity (or Ice-1) retracking scheme (Wingham *et al.* 1986; Bamber 1994) which is the best suited for hydrological applications (Frappart *et al.* 2006). For the ERS-2 data, we use the 20 Hz height from ERS-2 retracked with Ice-2 algorithm by the OSCAR project (Observations des Surfaces Continentales par Altimétrie Radar or Land Observations by Radar Altimetry) at LEGOS (Laboratoire d'Etudes en Océanographie Spatiale) in Toulouse (France). As of mid-2002, we use the ENVISAT data instead of ERS-2. Fig. 3 shows the ERS-2/ENVISAT track coverage over an Orthorectified Landsat Thematic Mapper Mosaic (https://zulu.ssc.nasa.gov/) of the study area. On Fig. 3 are also superimposed the few T/P tracks its 1992–2002 orbit. From 2002 September, a few months after the launch of its successor, Jason-1, T/P moved to a new orbit, midway between the former orbital tracks. We do not consider the latter data because of the too-short time-series available. For T/P, we use the GDRs (standard ocean data, AVISO database) which have been shown to be precise enough for continental water studies (e.g. Birkett 1998; Birkett *et al.* 2002; Maheu *et al.* 2003). The 10 yr (1992–2002) hydrological data set derived from T/P on its former orbit was expected to be extended with data from Jason-1. Unfortunately, Jason-1 provides too few land surface water measurements due to loss of surface lock by the onboard tracker and inaccurate retracking procedure over land surface waters. The T/P orbital cycle is 10 days. Compared to the 35 day orbit cycle of ERS/ENVISAT, this is obviously more favourable to study water level variations. But this is at the expense of the coverage which is very limited. The purpose of using also the T/P data here is mainly to assess the precision of the ERS-2 data at the crossing points between two tracks. In effect, several studies have assessed the T/P-based water level time-series by comparing with *in situ* gauges measurements (see below). Altimetry data of all satellites have been corrected for the classical geophysical and environmental corrections needed over land (instrumental, ionosphere, wet and dry troposphere, solid earth and pole tide corrections).

3.2 VEGETATION imagery

The VEGETATION (VGT) sensor, onboard SPOT-4 satellite, was designed to observe the vegetation and land surfaces (Arnaud & Leroy 1991). Since 1998 April, this sensor acquired data in four spectral bands: B0 (blue, 430–470 nm), B2 (red, 610–680 nm), B3 (near infrared, 780–890 nm) and SWIR (short-wave infrared, 1580–1750 nm). With a swath width of 2250 km, VGT provides daily coverage at 1 km spatial resolution. Three standard products are delivered to users: VGT-P (physical product), VGT-S1 (daily synthesis product) and VGT-S10 (10 day synthesis product). There are three 10 day composites for a month: day 1–10, day 11–20 and day 21 to the last day of the month. VGT-S10 products were obtained selecting the VGT-S1 value that have the maximum NDVI within a 10 day period. This product, known as maximum NDVI value composite (MVC), is used to minimize the effect of cloud cover and variability in atmospheric optical depth (Holben 1986). The NDVI, defined by

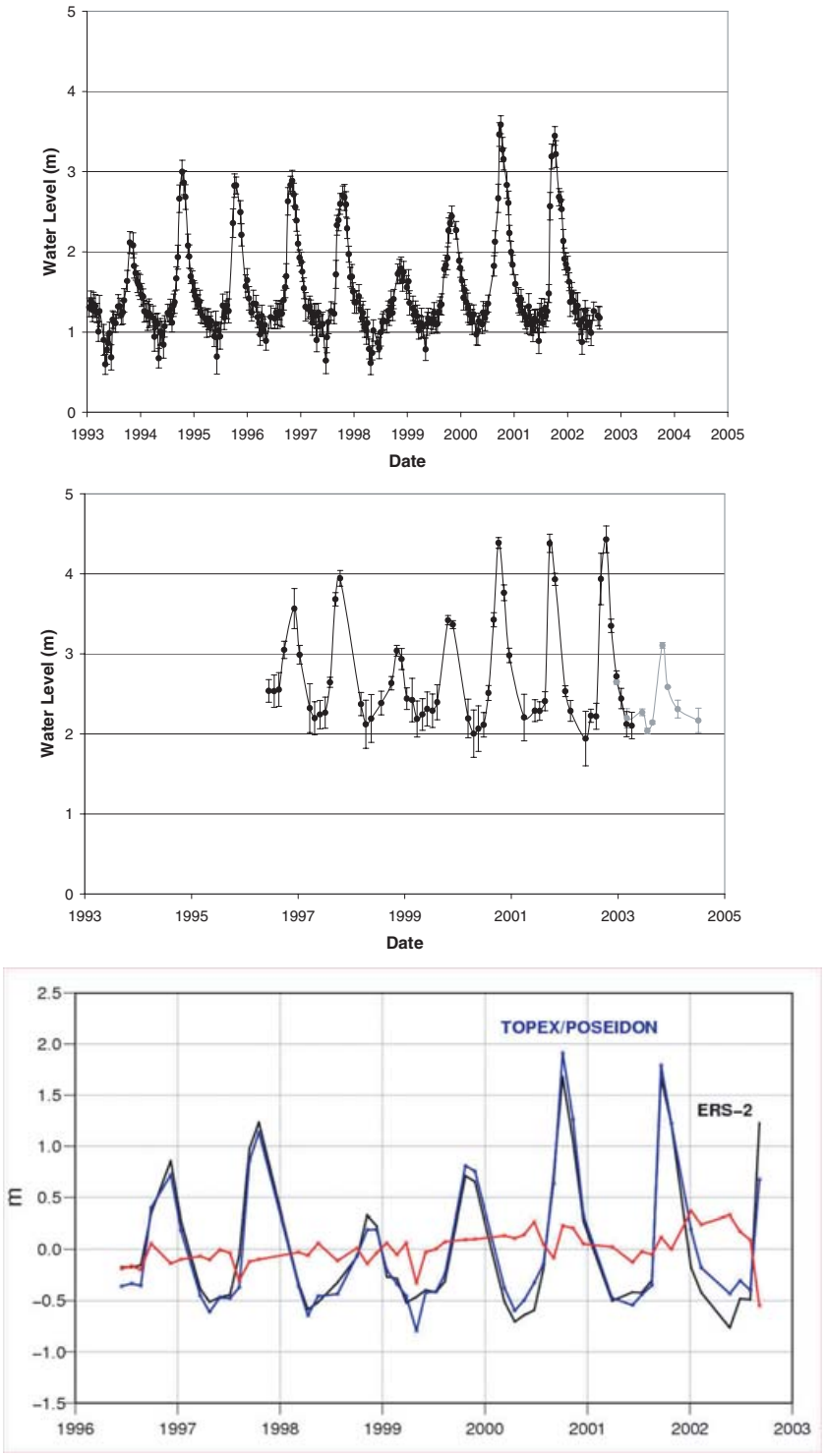

Figure 4. Comparison between T/P and ERS-2/ENVISAT-derived water level time-series. Upper panel: water level time-series and dispersion derived from T/P measurements, middle panel: water level time-series and dispersion derived from ERS-2/ENVISAT measurements (black and grey, respectively), lower panel: comparisons of the two water level anomalies (T/P in blue, ERS-2 in black) and residual difference (red curve). The continuous lines are simply joining the dots between the data points. The rms difference between *in situ* and altimetry-derived water levels are 0.23 m at Moc Hoa for ERS-2/ENVISAT and 0.15 m at Kg Luong for T/P.

Tucker (1979) is computed using the equation:

$$\mathrm{NDVI}_{\mathrm{VGT}} = \frac{B3 - B2}{B3 + B2}. \quad (1)$$

NDVI is primarily used to derive vegetation parameters for crop and forest monitoring, for the study of mass and biogeochemical cycles, and for assimilation in general circulation or weather forecast models (Duchemin *et al.* 2002).

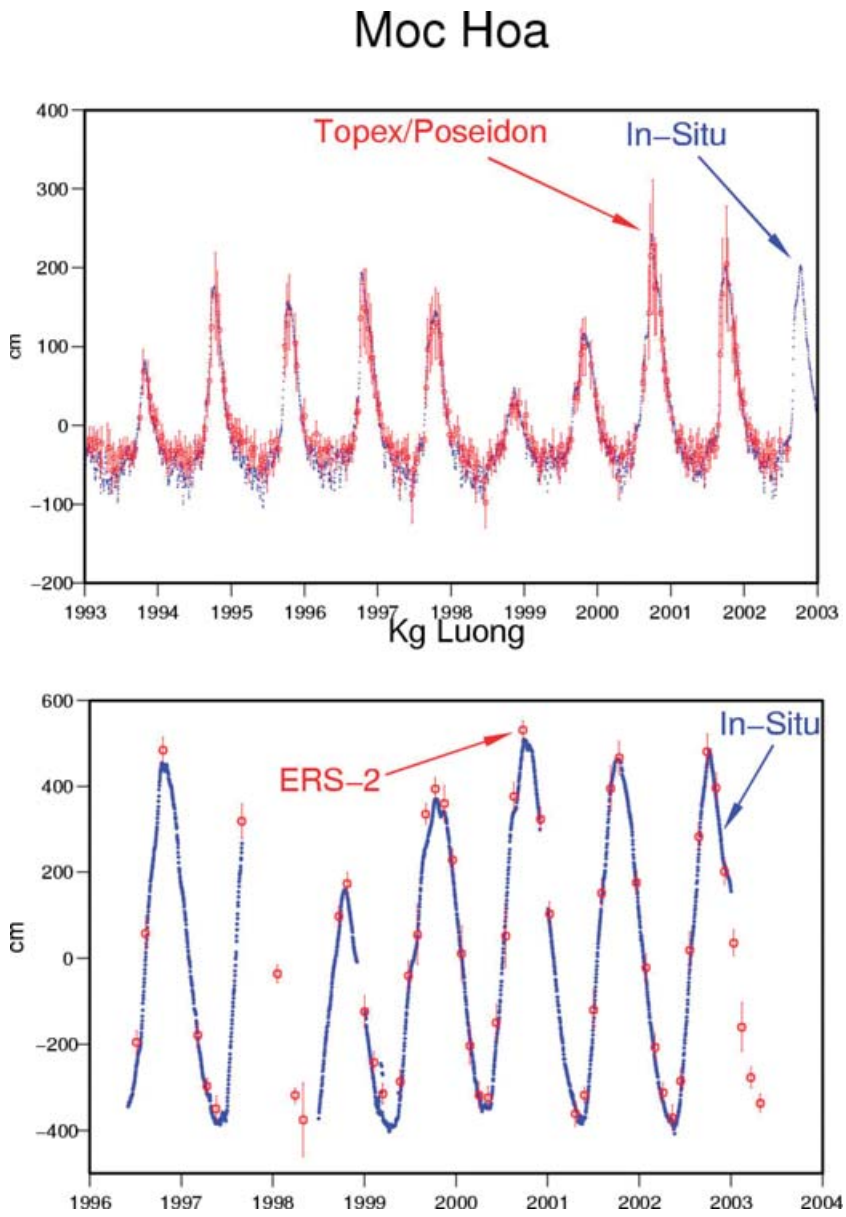

Figure 5. Comparison between altimetry-based and *in situ* water levels. Upper panel: T/P (red) versus Moc Hoa gauge station (blue) water levels. Lower panel: ERS-2 (red) versus Kg Luong gauge station (blue) water levels.

In this study, we use the VGT-S10 NDVI products from 1998 May to 2004 December available at http://free.vgt.vito.be/, to develop a method for mapping inundated areas.

4 WATER LEVEL TIME-SERIES

4.1 Altimetry-derived water levels

Along the satellite tracks shown in Fig. 3, we have considered 80 altimetry stations (called below virtual stations) at which we have computed water level time-series from the ERS-2 and ENVISAT altimetry data. These altimetry stations are identified in Fig. 3 by the white dots and yellow stars (the white dots correspond to total set of computed water level time-series while the yellow stars only correspond to those shown in Fig. 6). The virtual stations selected here are those which provide good quality water level time-series (according to the data editing and error bars associated to each time-series—see below) and data gaps. Most stations are located over the floodplains in the delta lowlands. Other stations correspond to intersections of the satellite tracks with the river. Finally, two stations are located on the Tonle Sap Lake. To construct a water level time-series, we consider all 20 Hz altimetry data along a portion of satellite track. The intersections between satellite tracks and rivers or floodplains are determined using an Orthorectified Landsat Thematic Mapper Mosaic (https://zulu.ssc.nasa.gov/) of 28.5 m resolution. Over rivers, the portion of satellite track considered corresponds to the river-satellite track intersection. Over floodplains, this portion ranges from 1 to ∼5 km. Once selected, the data are expressed in terms of water height (water level) above the geoid (for that purpose, the GRACE geoid GGM02C, complete to degree and order 150, has been used; Tapley *et al.* 2005). For each intersection between the river (or the floodplain) and the satellite ground track, we define a so-called 'virtual station', represented by a rectangular window. Outliers are deleted

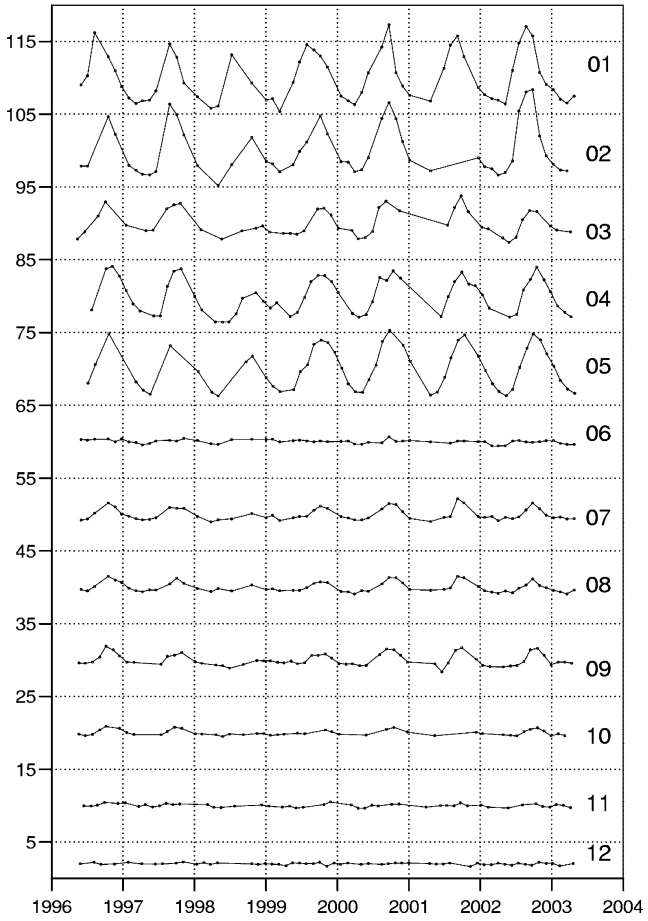

Figure 6. Examples of time-series of water level derived from ERS-2 in the lower Mekong basin (locations of sites 01 trough 12 are shown in Fig. 3). Sites 01–02 are main river, 03 is Tonle Sap river, 04–05 are Lake Tonle Sap, 06–09 are floodplain and 10–12 delta.

using a 3-σ criterion on the whole time span of analysis. For each 35 day cycle, the water level at a given virtual station is obtained by computing the median of all the high-rate data (20 Hz for ENVISAT and ERS-2 and 10 Hz for T/P) included in the rectangular window. This process, repeated for each cycle, allows the construction of a water level time-series at the virtual station.

The dispersion in L1 norm is given by the estimator known as median absolute deviation:

$$\mathrm{MAD}(x) = \frac{1}{N-1}\sum_{i=1}^{N} |x_i - x_{\mathrm{med}}|, \qquad (2)$$

where MAD(x): median absolute deviation of the observations, N: number of observations, x_i: ith observation, x_{med}: median of the observations.

4.2 Comparison of ERS-2/ENVISAT measurements with *in situ* gauge data and T/P time-series

The accuracy of T/P water level time-series over river and floodplains has been discussed in several previously published papers (i.e. Birkett 1998; de Oliveira Campos *et al.* 2001; Birkett *et al.* 2002; Maheu *et al.* 2003). Recently, validation of several tens of T/P-based water level time-series over rivers worldwide (through comparisons with *in situ* gauge data) indicates an average precision of about 30 cm (Cauhopé *et al.* 2006). Water levels derived from ERS-2/ENVISAT were only used in few studies (Berry *et al.* 2005; Frappart *et al.* 2006), indicating an averaged uncertainty of about 20 cm for ERS-2 and 15 cm for ENVISAT.

We have compared the water level time-series from ERS-2/ENVISAT with those from T/P at crossover points (intersections between the T/P and ERS-2/ENVISAT tracks). In Fig. 4(a) is presented an example of ERS-2 and T/P time-series at a crossover located in the floodplain (see the white open circle in Fig. 3). We present an example (Fig. 4a) of T/P, ERS-2 and ENVISAT time-series at a crossover in the floodplain (see the white ellipse in Fig. 3). In Fig. 4(a), the ERS-2 time-series has been completed by the ENVISAT data beyond mid-2002. Error bars are estimated as explained above. Fig. 4(b) presents the T/P-based and ERS-2 (ENVISAT)-based water level time-series at the crossover point after removing the mean to each time-series. The comparisons shown in Fig. 4(b) indicate that the ERS-2 time-series agrees very well with the T/P one, both in amplitude and phase. The difference between the two time-series is also presented in Fig. 4(b). The corresponding rms difference is 16 cm. This comparison allows us to quantify the precision of the ERS-derived water levels over the Mekong floodplain.

The water level time-series derived from radar altimetry were further compared with measurements from two *in situ* gauge stations (Moc Hoa and Kompong Luong—hereafter Kg Luong, pronounced Ky Luong—in Fig. 3). The Kg Luong station (104.20°, 12.56°), on the Tonle Sap Lake, is located 6 km upstream from an ERS-2/ENVISAT track and the Moc Hoa station (105.93°, 10.77°) is located 2 km away from a T/P track. The satellite and *in situ* water level time-series are, respectively, presented in Figs 5(a) and (b). Note only these two *in situ* gauge data sets were available over the study period in close vicinity of the satellite tracks. The rms difference between *in situ* and altimetry-derived water levels are, respectively, 0.23 and 0.15 m. The results obtained with ERS-2 on the Tonle Sap Lake are similar to those obtained by Mason *et al.* (1990) with Geosat, by Birkett & Mason (1995) with T/P and those presented by http://www.pecad.fas.usda.gov/ with T/P and Jason-1.

4.3 Analysis of the water level time-series

We have computed water level time-series at each of the 80 virtual stations. Since we cannot show all of them, we present in Fig. 6 a sample of these time-series corresponding to the virtual stations indicated by the yellow stars (from 1 to 12) in Fig. 3. Each time-series is artificially shifted by 10 m and error bars are not shown for clarity. The time-series numbered 1 and 2 are located on the main river upstream of the intersection with the Tonle Sap river. Both have a mean annual amplitude of about 10 m. The time-series numbered 3 is located on the Tonle Sap river. The two time-series 4 and 5 located on the Tonle Sap Lake (near the outlet) have a mean annual amplitude in the range 5–10 m peak to peak. Time-series 6 is almost flat. It is located over the lowlands floodplain in Vietnam. Time-series 7, 8, 9 also correspond to the lowlands floodplain. Their annual cycle has an amplitude of ∼2 m. A similar behaviour is noticed for all virtual stations of this area. The remaining three time-series of Fig. 6 (numbered 10, 11 and 12) are located in the delta, where the main river divides into several branches. All three have very small annual amplitude. We also note that the seasonal signal decreases into the delta where it almost disappears.

In order to get a synthesis of the water level change over the study area, we applied an EOF decomposition to the 80 water level time-series (Fig. 7). The principal component (temporal curve)

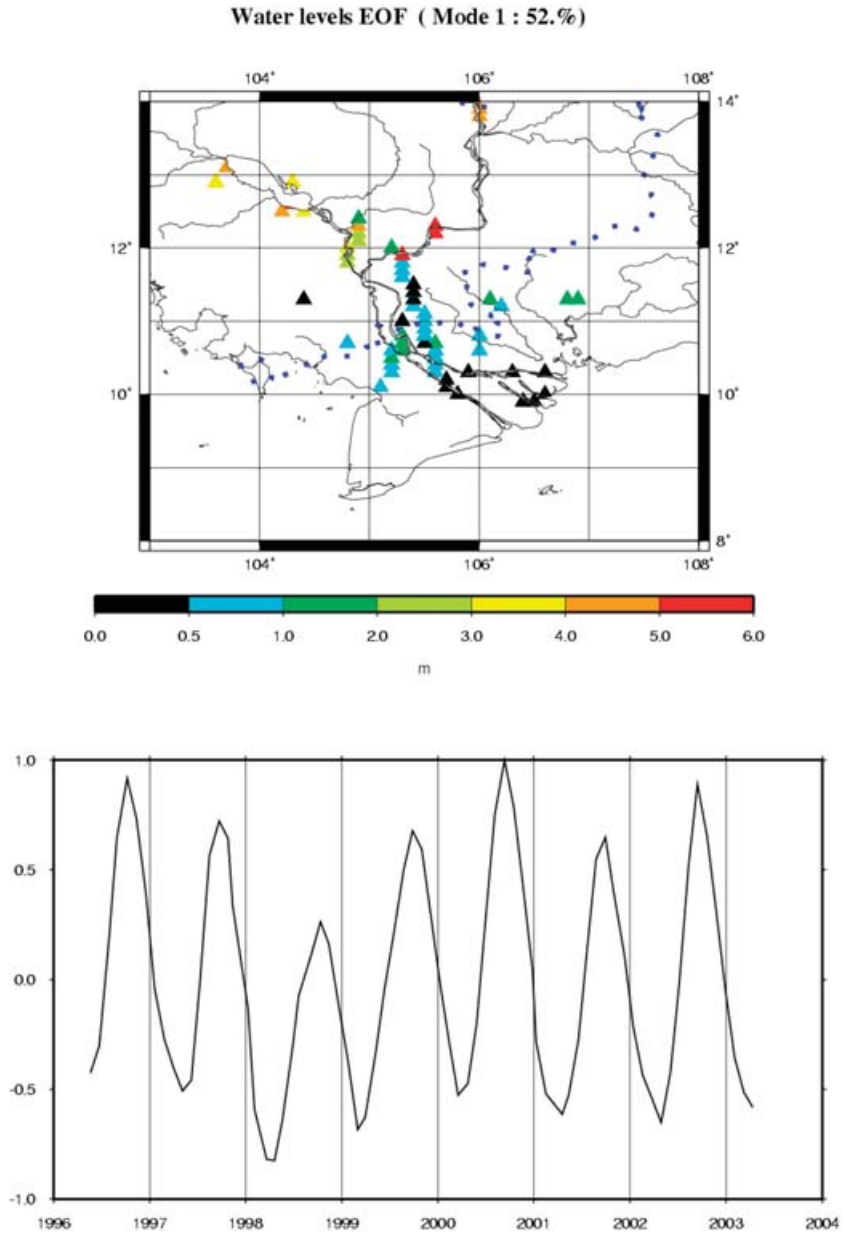

Figure 7. Mode 1 of the EOF decomposition of water levels derived from radar altimetry over the lower Mekong, between 1996 and 2003. The upper panel represents the spatial mode whereas the lower panel represents the temporal variations of the water levels derived from radar altimetry.

shows a minimum water level in year 1998 and a maximum in year 2000. The highest annual amplitudes (up to 10 m) are observed in the northern part of the studied region, upstream on the main river and in the Tonle Sap area. The lowlands floodplains display an annual water level cycle of about 2 m amplitude. Finally the lower delta does not exhibit any seasonal cycle.

5 INTERPOLATED WATER LEVEL MAPS

5.1 Delineation of the flood extent using SPOT-VGT

Among the numerous vegetation indices developed to monitor vegetation structure and activity, the NDVI is the most widely used. Over vegetation cover, NDVI values range in general from 0.3 to 0.8, depending on the vegetation density and photosynthetic activity. Over open water, the NDVI values are generally close to 0. The values of the pixels corresponding to identified water bodies (such as the Tonle Sap lake in Fig. 1) are about 0.1. However, NDVI has seldom been used to identify flooded area over land because of the presence in the pixel of partially submerged vegetation (trees, bushes and high crops), especially in the kilometre resolution pixels of SPOT-VGT or NOAA/AVHRR. In the Mekong delta, during the flood season, open water is found in a vast area of agricultural floodplains, dedicated mostly for rice. As an illustration, in Fig. 8(a) shows the time variations of NDVI for a specific region ($105.485^\circ <$ longitude $< 105.670^\circ$ and $10.559^\circ <$ latitude $< 10.698^\circ$) in the lowland floodplain. The NDVI variations correspond to two main crop cycles in the region, with maximum vegetation activity in April–May and December–January. From 2003 August to October, low values of NDVI should indicate the presence of open water over the region.

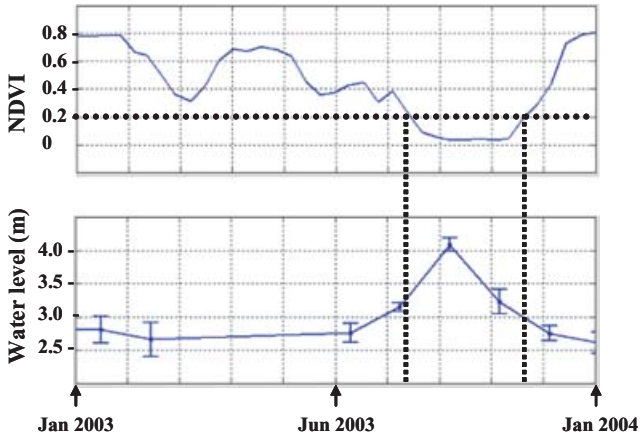

Figure 8. NDVI variations (top) between 2003 January and 2004 January of the region delimited by 105.485°E–105.670°E and 10.559N-10.698N, and available water level measurements at the virtual station within the region (bottom). The horizontal dashed line on the upper panel represents the threshold on NDVI we used to discriminate between flooded and non-flooded areas. The vertical dashed lines represent the corresponding time span.

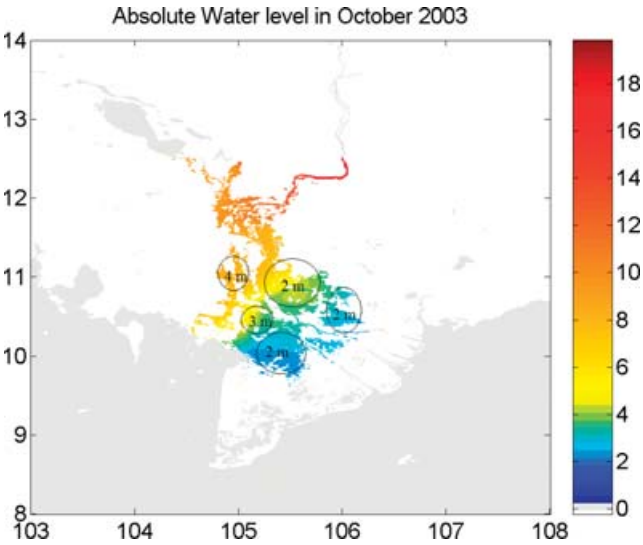

Figure 9. Location of the homogeneous altitude zones over the lower Mekong basin (black circles).

Fig. 8(b) shows the water level variations derived from ENVISAT altimetry. Values of the water level in August to October corroborate with the flooding observed by NDVI. An extensive sensitivity analysis indicates that the flooding conditions correspond to NDVI values between 0 and 0.35. A sensitivity analysis was undertaken on the whole study area, in the flood period from August to November. When the threshold in NDVI value changes between 0.15 and 0.25, the inundated area varies by 5 per cent. We assumed that the pixels that correspond to flooded areas have NDVI values lower than 0.2. The remaining uncertainty due to the NDVI threshold is expected to be not important in the analysis of the relative variation of the flooded area.

A second source of error is the presence of clouds which is likely to affect the delineation of the flooded zones in the Mekong basin. Cloud and poor atmospheric conditions generally depress NDVI values (Arino *et al.* 1992), and as a consequence, some non-inundated pixels are incorrectly considered as flooded. Although most of the cloudy pixels were eliminated by the maximum value composite (MVC) approach (Tarpley *et al.* 1984), a residual cloud contamination has been observed on some VGT-S10 products (Xiao *et al.* 2002). To reduce the effects of cloud contamination and atmospheric interference in seasonal NDVI time-series from daily AVHRR data, Viovy *et al.* (1992) developed the best index slope extraction (BISE) technique. It is based on the two following assumptions: (1) NDVI is depressed by cloud and atmospheric contamination and (2) rapid and non-persistent increases or decreases in NDVI are inconsistent with natural vegetation growth. Our method to discriminate between flooded and non-flooded but cloudy pixels is very similar to this developed by Viovy *et al.* (1992). We assume that: (1) NDVI is depressed by cloud and atmospheric contamination, (2) an inundated pixel remains inundated during several 10 day intervals (except at flood peak), and (3) during the flooded period (which occurs after the rainy season), pixels are rarely cloudy for two or more consecutive 10 day intervals. Hence, a pixel with a NDVI value lower than 0.2 during only one 10 day interval, is considered cloudy. This method has two main limitations: (1) if clouds are present on two or more consecutive 10 day intervals, the pixel can be wrongly considered inundated, and (2) some pixels on the boundary of the floodplains, inundated during only one 10 day interval can be discarded.

In each VGT-S10 image, we extract all the pixels whose value is finally lower than our threshold to produce 10 day flood maps. The monthly flood map is obtained as the union of the three 10 day flood maps and corresponds to the maximum extent of the flood during the month.

5.2 Monthly maps of interpolated surface water levels

Only one value of water level is available at each virtual station for a given month. The date of the water level measurements varies according to the location of the virtual station. For the ERS-2 period, some data are lacking during 1 month. We interpolate the water level between two consecutive months to complete the data set. As a consequence only monthly maps of water level can be estimated over the floodplain. At a given month during the flood, the altimetry-based water levels measured at the virtual stations were linearly interpolated over the flooded zones of the lower Mekong basin. Maps of interpolated surface water levels with 1 km resolution have been constructed for each month of the flood period, between July and December, for 1998–2003. ERS-2-derived surface water levels are used in the interpolation process for the period 1998–2002 and ENVISAT for 2003. As mentioned above, water levels are expressed with respect to the geoid. For the purpose of hydrological interpretation of water volumes, referring to the topography would be best as far as floodplains are concerned. However, available topographic databases are not necessarily precise enough for the present study. Altitude of the flooded region delineated by SPOT-VGT were derived from elevation points network in the 1/250 000 reference map of Vietnam (1986). Fig. 9 shows five subzones of homogeneous altitude from 2 to 4 m. The lower Mekong is thus mainly composed of large uniform zones (Fig. 9) where only month-to-month difference maps really represent water volume change (see below).

The monthly maps of water level were produced by bilinear interpolation scheme to estimate the water level for each grid point. South of 11°N, the Mekong river flows preferentially east–west. The ERS-2/ENVISAT tracks cross the river nearly perpendicularly, allowing clear separation of the contributions of the river mainstream from those of associated floodplains (see Fig. 3). As a consequence, the

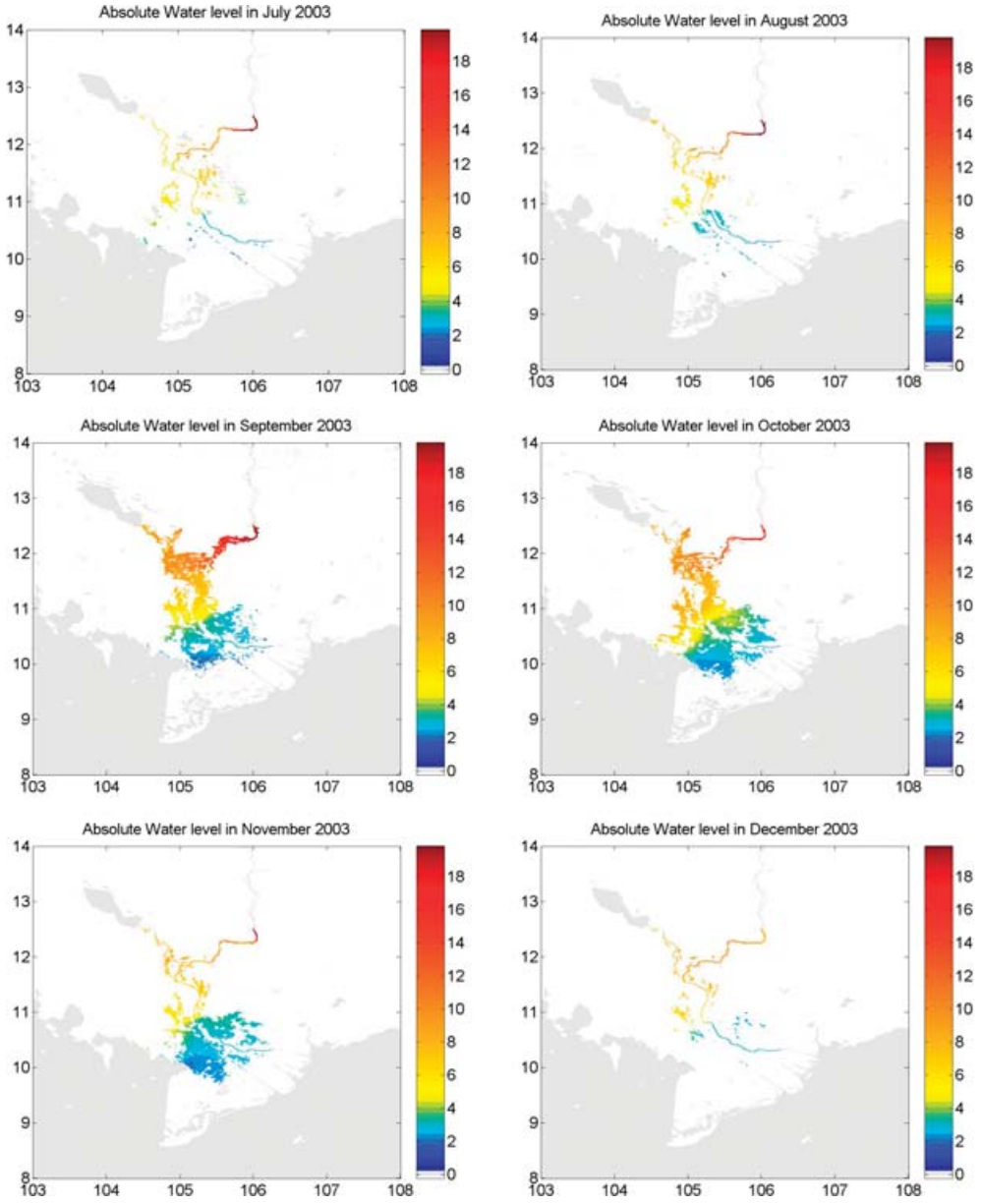

Figure 10. Altimetry-based water level maps (w.r.t. GRACE geoid) from 2003 July to December.

interpolation in the along-track direction follows the difference of water levels between the mainstream and the floodplain. In the cross-track direction, interpolation over several tens of kilometres will only reflect the mean slope of the river. Over the northern/southern flowing parts of the river network, the ERS-2/ENVISAT tracks run parallel to the river. In these cases, depending on the choice of the geographical coordinates of the virtual station, the time-series can be influenced by the elevation variation within the adjacent floodplain (Birkett *et al.* 2002). The latter authors did not report obvious amplitude or phase differences due to the inclusion of some floodplain. On the central floodplain, the network of virtual stations is sufficiently dense to avoid important interpolation errors.

The monthly flood maps indicate that the flood period generally ranges from September to November. As an example for year 2003, Fig. 10 shows maps of interpolated water levels between 2003 July and December. In July and August, limited flood is observed in the Mekong basin. In September, the upstream part of the Mekong basin is flooded. Water levels decrease in the upstream part of the Mekong river whereas they still rise in the Tonle Sap river between September and October. This situation corresponds to the flow reversal of the Tonle Sap river: during the flood, the water flows from the Mekong river to the Tonle Sap river whereas it flows from the Tonle Sap to the Mekong river when the water level decreases. The flood reaches the delta in October. The level of the Tonle Sap river decreases between November and October and the downstream part of the basin is inundated in November. The flood has ended in December and the situation is similar to the month of July.

Fig. 11 presents maps of water level differences for two couples of consecutive months (2003 October minus September) and (2003 November minus October). The sequence of events discussed above is even more visible in Fig. 12. Important variations in the extent of the flooded zone can be observed from one year to another. This can be shown in Fig. 12 which shows maps of interpolated water levels from the month of October for 1998–2003. Year 2000 is

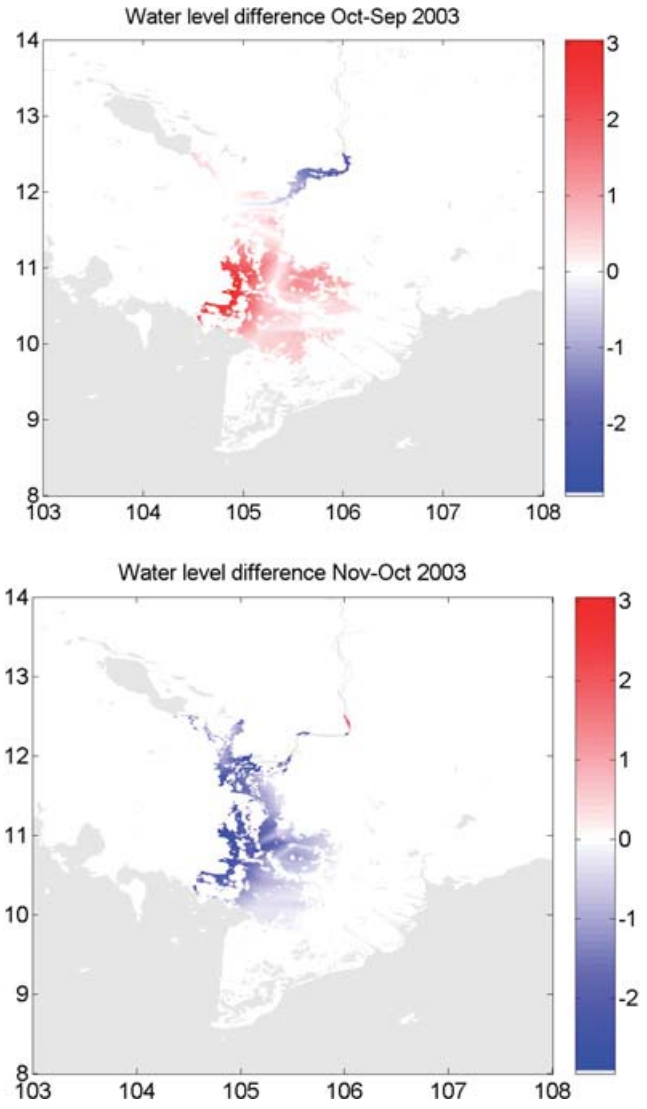

Figure 11. Altimetry-based water level difference maps: 2003 October minus September and 2003 November minus October (m). The flood reaches the delta in October. The level of the Tonle Sap river decreases between November and October and the downstream part of the basin is inundated in November. The flood ended in December and the situation is similar to the month of July.

characterized by an exceptionally long flood period, from August to December, as was reported by Dutta & Takeuchi (2000) and Chia *et al.* (2001). The maximum extent is reached in 2000, and years 2001 and 2002 present large floods compared with years 1998, 1999 and 2003.

6 WATER VOLUME VARIATIONS

6.1 Surface water volume change

Determining the temporal variation of water volume stored in the floodplains has many applications in hydrology. For the inundated areas permanently or temporarily connected to main channels, the determination of the water volume variation is equivalent to the estimation of water volume potentially stored and/or released by the valley reach during flood stages. The water volume variation in this type of inundated area is an important parameter for the hydrodynamic modelling of the river flow and the determination of its transport capacity. For the inundated areas that never connect to the main channel, the volume variation is essentially a function of the base flow variation, the inputs from the local basin and the rain. Some floodplains present both types of flooding zones. Areas where the river water mixes with the local water are called 'perirheic zones' (Mertes 1997). In all cases, the inundation area is a buffer zone between the river and the upland watershed. The water volume variation represents the flood pulse of floodplains as expressed by Junk *et al.* (1989). Therefore, it is a key ecological characteristic that cannot be easily measured in the field.

The variation of water volume corresponds to the surface water levels difference integrated over the inundated surface. These variations $\delta V(t_i, t_{i-1})$, between two consecutive months numbered i and $i-1$, over the floodplain S is the sum of the products of the difference of surface water levels $\delta h_j(i, i-1)$, with $j = 1, 2, \ldots$ inside S, by the elementary surfaces $R_e^2\,\delta\lambda\,\delta\theta\,\sin\theta_j$:

$$\delta V(i, i-1) = R_e^2 \delta\lambda\,\delta\theta \sum_{j\in S} \delta h_j(\theta, \lambda, i, i-1)\sin(\theta j), \tag{3}$$

where $\delta\,\lambda$ and $\delta\theta$ are the sampling grid steps along longitude and latitude ($\sim 0.01^\circ$), respectively, and R_e the mean radius of the Earth ($\sim$6378 km). The surface water volume variations are expressed in km^3/month.

The error on the method was estimated using:

$$d\delta V = \sum_{i=1}^{n} (dS_i \delta h_i + S_i d\delta h_i), \tag{4}$$

where: $d\delta V$ is the error on the water volume variation (δV), S_i is the ith elementary surface and δh_i is the ith elementary water level variation between two consecutive months, dS_i is the error on the ith elementary surface, $d\delta h_i$ is the error on the ith elementary water level variation between two consecutive months.

The maximum error on the volume variation can be estimated as:

$$\Delta(\delta V_{\max}) \leq \Delta S \max \delta h_{\max} + S_{\max}\Delta(\delta h_{\max}), \tag{5}$$

where: $\Delta(\delta V_{\max})$ is the maximum error on the water volume variation (δV), $S_{\max}$ is the maximum flooded surface, $\delta h_{\max}$ is the maximum water level variation between two consecutive months, $\Delta S_{\max}$ is the maximum error on the flooded surface, $\Delta(\delta h_{\max})$ is the maximum error on the water level variation between two consecutive months.

Using eq. (5), we have estimated the maximum error on the volume change in the lower Mekong basin with the following values:

(i) $S_{\max} = 45\,000$ km^2 in year 2000 (MRC 2005),
(ii) $\delta h_{\max} = 2$ m,
(iii) $\Delta S_{\max} = 5$ per cent of 45 000 km^2,
(iv) $\Delta\,(\delta h_{\max}) = 0.25$ m.

For the whole study zone, we obtained a maximum error of 16 km^3 for the year 2000 for a total positive variation of 32.8 km^3.

Fig. 13 presents the differences between two consecutive months of the mean water volume averaged over the study area for 1996–2003. Only months from August to December are considered. Positive variations are obtained between August and October. They are more important for the years 2000, 2001, 2002 than for 1998, 1999 and 2003, with volume variations greater than 15 km^3 and reaching 25 km^3 between 2002 September and August. The important flood of 2000 can be related to the exceptional precipitation event

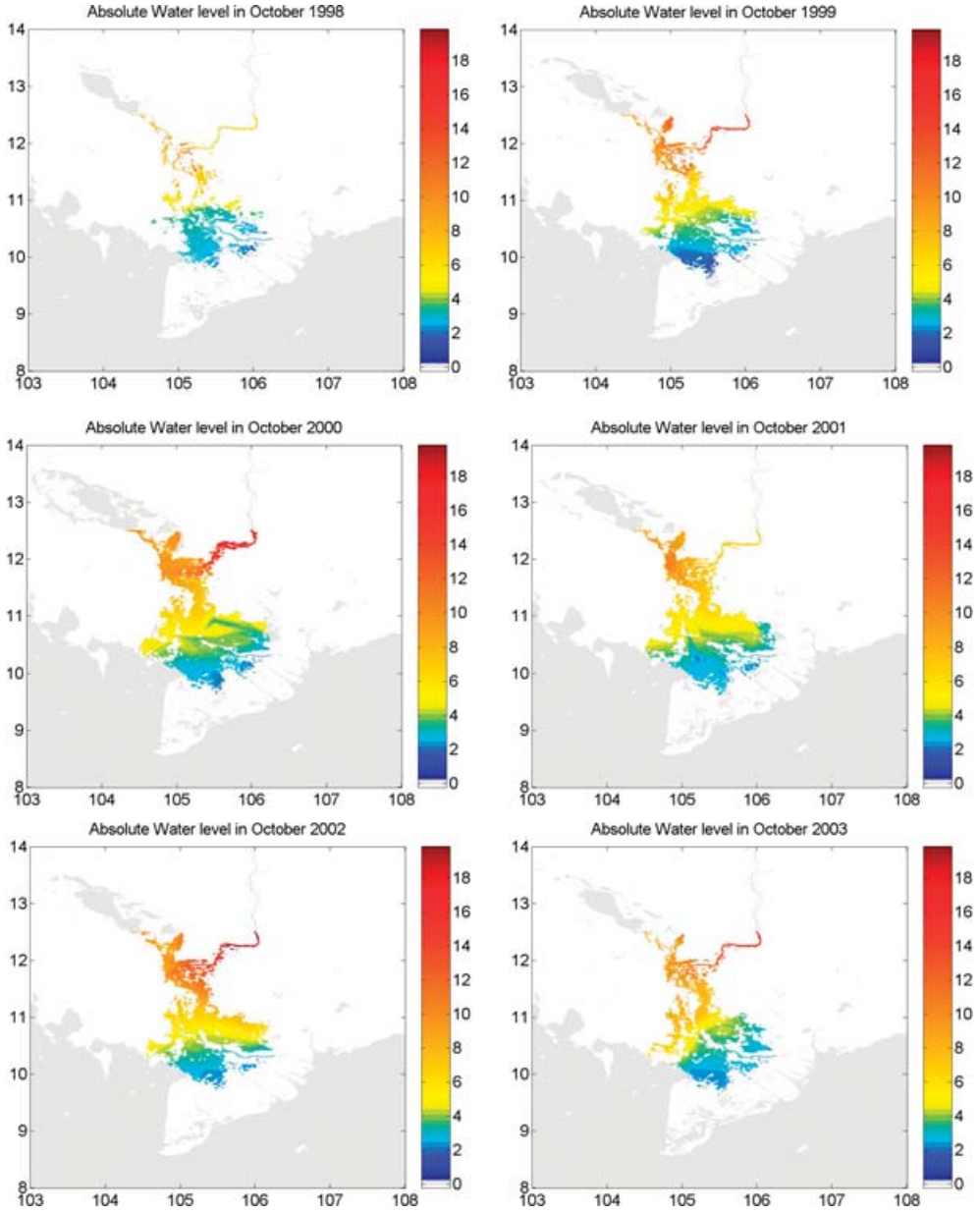

Figure 12. Altimetry-based water level maps (w.r.t. GRACE geoid) for 1998 October to 2003 at the maximum of the flood.

(see Fig. 2). No similar events can be invoked to explain the great floods of 2001 and 2002.

6.2 Comparison with the total water volume change determined by GRACE

The GRACE mission, launched in 2002 March, is devoted to measure spatio-temporal change of the gravity that results mainly from water mass redistribution among the surface fluid envelops (Tapley *et al.* 2004a). Several recent studies have shown that GRACE data over the continents provide important new information on the total land water storage (surface waters, soil moisture and underground waters, and where appropriate on snow mass) (Tapley *et al.* 2004b; Wahr *et al.* 2004; Chen *et al.* 2005; Schmidt *et al.* 2006; Ramillien *et al.* 2005). Wahr *et al.* (2004) estimated the error on the land water storage to be ∼18 mm for a 750 km spatial average GRACE-based land water solutions. (Ramillien *et al.* 2005, 2006) found an error ∼15 mm as the final *a posteriori* uncertainties on the land water solutions, with spatial resolution of 660 km. Ramillien *et al.* (2005) computed monthly change in total water mass volume in several different river basins, including the Mekong. In Fig. 10, we present the difference between two consecutive months of the vertically integrated water volume change from GRACE over the whole Mekong basin for the period 2002 May–2004 April. Comparing with monthly differences in surface water volume change computed in the present study, we note that the GRACE-derived total water volume differences display almost in-phase seasonal fluctuations. The agreement is particularly good during periods of water falling and around minimum water level. It should be recalled, however, that GRACE provides the sum of surface waters and soil/underground waters. In addition, due to the current GRACE spatial resolution (∼600 km), the land water storage has been computed over the whole Mekong basin, an area much larger than that considered in

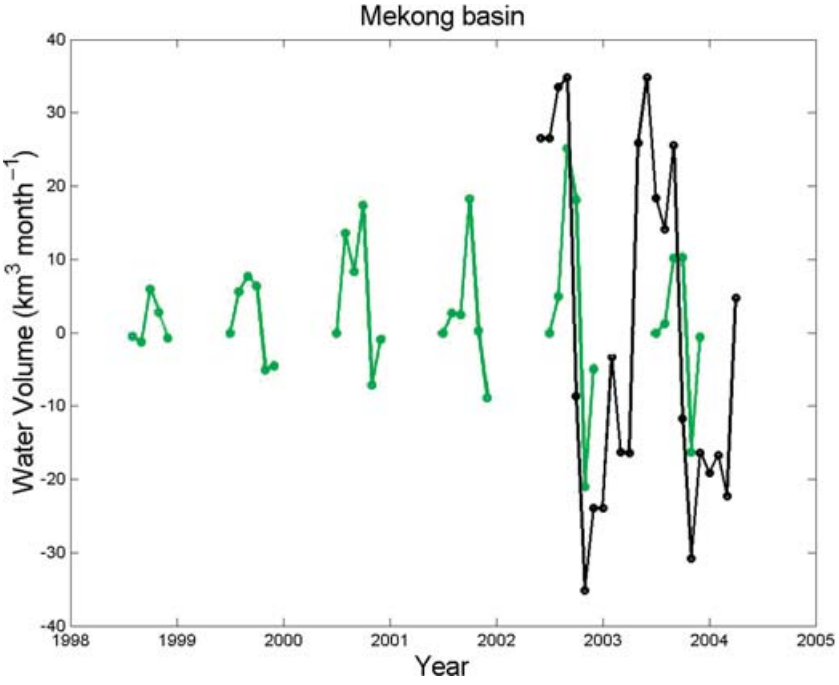

Figure 13. Variation of surface water volume from ERS-2/ENVISAT altimetry and SPOT-VGT imagery (green) and total land water volume from GRACE (black).

the present study. However, this comparison shows that in the future when the GRACE resolution will improve, it could be possible to combine the GRACE result with the water volume change inferred from altimetry data to extract the subsurface water storage change.

7 CONCLUSIONS

This study shows that the rather dense coverage of ERS-2/ENVISAT satellites (compared to T/P) over the Mekong floodplains allows us to describe the geographical variations in seasonal high/low water levels. Accuracies of 15 of 23 cm were found for T/P and ERS-2, respectively, by comparisons between altimetry-derived water levels and *in situ* gauge measurements. In particular we noticed a strong difference between the northern part of the Lower Mekong (upstream of the intersection between the main river and the Tonle Sap river, as well as the Tonle Sap region) and the southern part which includes the main floodplain and delta. The latter exhibits very small seasonal fluctuations (less than 2 m) compared to the former (up to 10 m). This may possibly result from the many canals and dams built during the last two decades in the floodplain area.

This study also demonstrates that combining dense altimetry-based water levels with satellite imagery (here NDVI data from the SPOT-4/Vegetation instrument) provides a new method for remotely measuring surface water volumes over large floodplains. This combination provides valuable information on the dynamics of the inundation of river floodplains. Important interannual variations were observed both in extent and volume over the 1998–2003 period. Knowledge of surface water volumes has several potential applications, for example flood monitoring and forecasting, or sediment transport assessment. In the near future, when GRACE observations will improve in terms of geographical resolution, it will be possible to estimate change in water volumes stored in soil and underground reservoirs by using in synergy GRACE, altimetry and imagery data. Separation of deep and surface land water contributions can also be of interest in global/regional land surface model validation.

ACKNOWLEDGMENTS

The authors acknowledge the AVISO data centre at CNES and the NASA Physical Oceanography DAAC for the T/P data and THE ESA for the ERS-2/ENVISAT data. We thank B. Legrésy for having made available to us retracked ERS-2 altimetry data. We also acknowledge the Centre de Topographie des Océans et de l'Hydrosphère (CTOH) at LEGOS for providing us with the T/P and ENVISAT data. We express our gratitude to Dr John Beavan for reviewing the English of the paper. One of us (FF) was supported by a CNES/ALCATEL PhD grant.

REFERENCES

Alsdorf, D.E., Melack, J.M., Dunne, T., Mertes, L.AK., Hess, L.L. & Smith, L.C., 2000. Interferometric radar measurements of water level changes on the Amazon floodplain, *Nature,* 404, 174–177.

Alsdorf, D.E., Smith, L.C. & Melack, J.M., 2001. Amazon floodplain water level changes measured with interferometric SIR-C radar, *IEEE Trans. Geosci. Remote Sensing,* 39(2), 423–431.

Arino, O., Dedieu, G. & Deschamps, P., 1992. Determination of satellite land surface reflectances using METEOSAT and NOAA/AVHRR shortwave channel data, *Int. J. Remote Sensing,* 13, 2263–2287.

Arnaud, M. & Leroy, M., 1991. SPOT 4: a new generation of SPOT satellites, *ISPRS Journal of Photogrammetry and Remote Sensing,* 46, 205–215.

AVISO, 1996. *AVISO User Handbook: Merged TOPEX/POSEIDON Products,* AVI-NT-02–101-CN, 3rd ed, CNES, Toulouse, France, 194 pp.

Bamber, J.L., 1994. Ice sheet altimeter processing scheme, *Int. J. Remote Sensing,* 15(4), 925–938.

Berry, P.A.M., Garlick, J.D., Freeman, J. A. & Mathers, E.L., 2005. Global inland water monitoring from multi-mission altimetry, *Geophys. Res. Lett.,* 32, L16401, doi:10.1029/2005GL022814.

Birkett, C.M. & Mason, I.M., 1995. A new Global Lakes Database for a remote sensing programme studying climatically sensitive large lakes, *J. of Great Lakes Research,* 21(3), 307–318.

Birkett, C.M., 1998. Contribution of the TOPEX NASA radar altimeter to the global monitoring of large rivers and wetlands, *Water Resour. Res.,* 34(5), 1223–1239.

Birkett, C.M., Mertes, L. A. K., Dunne, T., Costa, M.H. & Jasinski, M.J., 2002. Surface water dynamics in the Amazon Basin: application of satellite radar altimetry, *J. geophys. Res.,* 107(D20), 8059–8080.

Cauhopé, M., Gennero, M. C., DoMinh, K., Cretaux, J.F., Berge-Nguyen, M., Cazenave, A. & Seyler, F., 2006. Worldwide validation of satellite altimetry-based water level time series, *EGU06-A-02342, HS52,* EGU General Assembly 2006, 02–07 April 2006 Wien (Austria).

Chen, J.L., Wilson, C.R., Famiglietti, J.S. & Rodell, M., 2005. Spatial sensitivity of the Gravity Recovery and Climate Experiment (GRACE) time-variable gravity observations, *J. Geophys. Res., Solid Earth,* 110, B08408.

Chia, A.S., Chen, P. & Liew, S.C., 2001. Flood extent in the Lower Mekong Basin evaluated using SPOT Quicklook mosaics, *22nd Asian Conference on Remote Sensing,* 5–9 November 2001.

Coe, M.T., Costa, M.H., Botta, A. & Birkett, C.M., 2002. Long term simualtions of discharge and floods in the Amazon Basin, *J. geophys. Res.,* 107(D20), 10 129–10 146.

Dow, J.M., Martinez Fadrique, F.M. & Zandbergen, R., 1999. High precision altimetry from the ENVISAT mission, *Adv. Space Res.,* 23(4), 757–762.

Duchemin, B., Berthelot, B., Dedieu, G., Leroy, M. & Maisongrande, P., 2002. Normalisation of directional effects in 10-day global syntheses derived from VEGETATION/SPOT: II. Validation of an operational method on actual datasets, *Remote Sens. Env.,* 81, 101–113.

Dutta, D. & Takeuchi, K., 2000. A report on the devastating floods in Cambodia, Report, International Center for Disaster-Mitigation and Engineering (INCEDE), Institute for Industrial Science, University of Tokyo.

ESA, 2002. ENVISAT RA2/MWR Product Handbook, *RA2/MWR Products User Guide*.

Frappart, F., Seyler, F., Martinez, J.M., Leòn, J.G. & Cazenave, A., 2005. Floodplain Water Storage in the Negro River Basin Estimated from Microwave Remote Sensing of Inundation Area and Water Levels, *Remote Sens. Env.,* 99, 387–399.

Frappart, F., Calmant, S., Cauhopé, M., Seyler, F. & Cazenave, A., 2006. Preliminary results of ENVISAT RA-2 derived water levels validation over the Amazon basin, *Remote Sens. Environ.,* 100, 252–264.

Gardini, B., Graf, G. & Ratier, G., 1995. The instruments on ENVISAT, *Acta Astronautica,* 37, 301–311.

Hamilton, S.K., Sippel, S.J. & Melack, J.M., 2002. Comparison of innundation patterns among major South American floodplains, *J. geophys. Res.,* 107(D20), 10.129–10.143.

Hess, L.L., Melack, J.M., Novo, E.M.L.M., Barbosa, C.C.F. & Gastil, M., 2003. Dual-season mapping of wetland inundation and vegetation for the central Amazon basin, *Remote Sens. Environ.,* 87(4), 404–428.

Hoanh, C.T., Guttman, H., Droogers, P. & Aerts J., 2003. Water, climate, food, and environment is the Mekong basin in southeast Asia, *Contribution to project ADAT, Adaptation strategies to changing environments, Final report,* 58 pp.

Holben, B.N., 1986. Characteristics of maximum-value composite images from temporal AVHRR data, *Int. J. Remote Sensing,* 7, 1417–1434.

Hori, H., 2000. *The Mekong Environment and Development,* the United Nations University, New York USA.

Interim Mekong Committee, 1988. Perspectives for Mekong Development. Revised indicative plan (1987) for the development of land, water and related resources of the lower Mekong basin. Committee report. Interim Committee for Coordination of Investigations of the lower Mekong Basin, Bangkok, Thailand.

Junk, W., Bayley, P.B. & Sparks, R.E., 1989. The flood pulse concept in river floodplain systems, in *Proceedings of the International Large River Symposium. Can. Spec. Pub. Fish. Aquat. Sci.,* Vol.106, pp. 110–127. ed. Dodge, D. P.

Kite, G., 2001. Modelling the Mekong: hydrological simulation for environmental impact studies, *J. Hydro.,* 253, 1–13.

Laxon, S., 1994. Sea ice altimeter processing scheme at the EODC, *Int. J. Remote Sensing,* 15(4), 915–924.

Legrésy, B., 1995. Etude du retracking des surfaces des formes d'onde altimétriques au-dessus des calottes, *rapport CNES, CT/ED/TU/UD96.188, contrat n° 856/2/95/CNES/006,* 81 pp.

Maheu, C., Cazenave, A. & Mechoso, C.R., 2003. Water level fluctuations in the Plata basin (South America) from Topex/Poseidon satellite altimetry, *Geophys. Res. Let.,* 30(3), 1143–1146.

Mason, I.M., Harris, A., Birkett, C.M., Cudlip, W. & Rapley, C.G., 1990. Remote sensing of lakes for the proxy monitoring of climatic change, in *Remote Sensing and Global Change, Proceedings of the 16th Annual Conference of the Remote Sensing Society,* 314–324.

Mertes, L.A.K., 1997. Documentation and significance of the perirheic zone on inundated floodplains, *Water Resour. Res.,* 33(7), 1749–1762.

Mertes, L.A.K., Daniel, D.L., Melack, J.M., Nelson, B., Martinelli, L.A. & Forsberg, B.R., 1995. Spatial patterns of hydrology, geomorphology, and vegetation on the floodplain of the Amazon River in Brazil from remote sensing perspective, *Geomorphology,* 13, 215–232.

Mekong River Commission and United Nations Environment Programme, 1997. Mekong River Basin diagnostic study. Final report. Mekong River Commission (MRC), Pnomh Penh, Cambodia.

Mekong River Commission, 2002. Annual report. Mekong River Commission (MRC) Secretariat, Pnomh Penh, Cambodia.

Mekong River Commission, 2003. Water, Climate, Food and Environment in the Mekong basin in southeast Asia, Final report, Mekong River Commission (MRC) Secretariat, June 2003.

Mekong River Commission, 2005. Overview of the Hydrology of the Mekong Basin, Mekong River Commission, Vientiane, November 2005, 73 pp.

de Oliveira Campos, I., Mercier, F., Maheu, C., Cochonneau, G., Kosuth, P., Blitzkow, D. & Cazenave A., 2001. Temporal variations of river basin waters from Topex/Poseidon satellite altimetry; application to the Amazon basin, *C.R. Acad. Sci. Paris, Sciences de la Terre et des planètes,* 333, 1–11.

Ramillien, G., Frappart, F., Cazenave, A. & Güntner, A., 2005. Time variations of the land water storage from an inversion of 2 years of GRACE geoids, *Earth planet. Sci. Lett.,* 235, 283–301.

Ramillien, G., Frappart, F., Güntner, A., Ngo-Duc, T., Cazenave, A. & Laval, K., 2006. Time variations of the regional evapotranspiration rate from GRACE satellite gravimetry, *Water Resour. Res.,* in press.

Rudolf, B., Hauschild, H., Rueth, W. & Schneider, U., 1994. Terrestrial precipitation analysis: operational method and required density of point measurements, in *Global Precipitations and Climate Change,* Vol. 26, pp. 173–186. ed. Desbois, M. & Desalmond, F., NATO ASI Series I, Springer-Verlag.

Rudolf, B., Fuchs, T., Schneider, U. & Meyer-Christoffer, A., 2003. Introduction of the Global Precipitation Climatology Centre (GPCC), Deutscher Wetterdienst, Offenbach a.M.; p. 16.

Schmidt, R. *et al.*, 2006. GRACE observations of changes in continental water storage, *Glob. And Plan. Change,* 50, 112–126.

Sippel, S.J., Hamilton, S.K., Melack, J.M. & Novo, E.M.M., 1998. Passive microwave observations of inundation area and the area/stage relation in the Amazon River floodplain, *Int. J. Remote Sens.,* 19, 3055–3074.

Smith, L.C., 1997. Satellite remote sensing of river innundation area, stage and discharge: a review, *Hydrol. Process.,* 11, 1427–1439.

Tanaka, M., Sugimura, T., Tanaka, S. & Tamai, N., 2003. Flood-drought cycle of Tonle Sap and Mekong Delta area observed by DMSP-SSM/I, *Int. J. Remote Sens.,* 24(7), 1487–1504.

Tapley, B.D., Bettadpur, S., Watkins, M. & Reigber, C., 2004a. The Gravity Recovery and Climate Experiment: Mission overview and Early results, *Geophys. Res. Lett.,* 31, L09607, doi:10.1029/2004GL019920.

Tapley, B.D., Bettadpur, S., Ries, J.C., Thompson, P.F. & Watkins, M., 2004b. GRACE measurements of mass variability in the Earth system, *Science,* 305, 503–505.

Tapley, B. *et al.*, 2005. GGM02—an improved Earth gravity field model from GRACE, *J. Geod.,* 79, doi:10.1007/s00190-005-0480-z, 467–478.

Tarpley, J.P., Schneider, S.R. & Money, R.L., 1984. Global vegetation indices from NOAA-7 meteorological satellite, *J. Climate and Applied Meteorology,* 23,491–494.

Toumazou, V. & Crétaux, J.F., 2001. Using a Lanczos eigensolver in the computation of Empirical Orthogonal Functions, *Monthly Weather Review,* 129(5), 1243–1250, doi:10.1175/1520–0493.

Töyrä, J., Pietroniro, A. & Martz, L.W., 2001. Multisensor hydrologic assessment of a freshwater wetland, *Remote Sens. Environ.,* 75,162–173.

Tucker, C.J., 1979. Red and photographic infrared linear combinations for monitoring vegetation, *Remote Sens. Env.,* 8,127–150.

Viovy, N., Arino, O. & Belward, A.S., 1992. The Best Index Slope Extraction (BISE): A method for reducing noise in NDVI time-series, *Int. J. Remote Sensing,* 13(8), 1585–1590.

Wehr, T. & Attema, E., 2001. Geophysical validation of ENVISAT data products, *Adv. Space Res.,* 28(1), 83–91.

Wahr, J., Molenaar, M. & Bryan, F., 1998. Time-variability of the Earth's gravity field: hydrological and oceanic effects and their possible detection using GRACE, *J. geophys. Res.,* 103,30 205–30 230.

Wahr, J., Swenson, S., Zlotnicki, V. & Velicogna, I., 2004. Time-variable gravity from GRACE: first results, *Geophys. Res. Let.,* 31,L11501.

Wingham, D.J., Rapley, C.G. & Griffiths, H., 1986. New techniques in satellite altimeter tracking systems, *Proceedings of IGARSS'86 Symposium, Zürich,* 8–11 September 1986, Ref. ESA SP-254, 1339–1344.

Xiao, X., Boles, S., Liu, J., Zhuang, D. & Liu, M., 2002. Characterization of forest type in northeastern China, using multi-temporal SPOT-4 VEGETATION sensor data, *Remote Sens. Env.,* 82,335–348.

Zelli, C., 1999. ENVISAT RA-2 advanced radar altimeter: instrument design and pre-launch performance assessment review, *Acta Astronautica,* 44, 323–333.